THE JOURNAL OF PHYSICAL CHEMISTRY A

ARTICLE

pubs.acs.org/JPCA

Time-Dependent Fifth-Order Bands in Nominally Third-Order 2D IR Vibrational Echo Spectra

Megan C. Thielges and Michael D. Fayer*

Department of Chemistry, Stanford University, Stanford, California 94305, United States

Supporting Information

ABSTRACT: Progress in the field of 2D IR vibrational spectroscopy has been bolstered by the production of intense mid-IR laser pulses. As higher-energy pulses are employed, a concomitant increase occurs in the likelihood of fifth-order contributions to the 2D IR spectra. We report the appearance of fifth-order signals in 2D IR spectra of CO bound to the active site of the enzyme cytochrome $P450_{cam}$ with the substrate norcamphor. Two bands with novel time dependences, one on the diagonal and one off-diagonal, are not accounted for by normal third-order interactions. These bands are associated with a $\nu = 1-2$ vibrational transition frequency. Both bands decay to 0 and then grow back in with opposite sign. The diagonal band is positive at short time, decays to 0, reappears with negative sign, before eventually decaying to 0. The off-diagonal band is negative at short time, decays to 0, reappears positive, and then decays to 0. The appearance and time dependence of these bands are characterized. Understanding these fifth-order bands is useful because they may be misidentified with time-dependent bands that arise from other processes, such as chemical exchange, vibrational coupling, or energy transfer. The presence and unusual time dependences of the fifth-order bands are reproduced with model calculations that account for the fact that vibrational relaxation from the $\nu = 2$ to 1 level is approximately a factor of 2 faster than that from the $\nu = 1$ to 0 level.

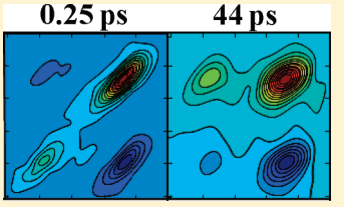

1. INTRODUCTION

Two-dimensional infrared (2D IR) vibrational echo studies of proteins and other condensed matter systems are becoming increasingly prevalent.[1−19] While vibrational spectra are highly sensitive to molecular environment and structure, those of condensed-phase systems are often congested with multiple overlapping inhomogeneously broadened bands. 2D IR spectra enhance spectral resolution by spreading out the frequency axis, permit accurate measurement of anharmonicities, and reveal couplings among vibrations.[1−3] Analysis of time-dependent 2D IR spectral line shapes reveal the dynamics of the vibrational oscillator's surrounding environment.[4−6] The time evolution of the 2D spectral line shapes has been particularly useful for studying fast dynamics on the ground electronic state under thermal equilibrium conditions. In addition, the time dependence of the appearance of off-diagonal bands in 2D IR spectra can reveal the rates of chemical exchange processes,[7−11] changes in coupling among vibrations,[12] or vibrational energy flow within molecules.[13]

A conventional vibrational echo experiment is a third-order technique that involves the intersection of three separately delayed pulses in a sample and selective detection of the vibrational echo signal, which is emitted in a unique direction determined by the phase-matching geometry. Combining the vibrational echo with another pulse, called the local oscillator, provides heterodyne detection that amplifies the vibrational echo. In addition to amplification, the heterodyne-detected signal provides phase information, which is necessary to perform Fourier transformations of the data to produce full 2D IR spectra. Although heterodyne detection amplifies the emitted echo, the nonlinear nature of the experiment combined with the typically small vibrational transition dipoles leads to weak signals. The emitted echo amplitude is linear in the electric field of each excitation pulse; therefore, it varies as $I^{3/2}$ of the initial IR pulse prior to splitting into the excitation pulses. Therefore, high-intensity excitation pulses are used to enhance the signal-to-noise ratio. At third-order, there is one electric field interaction between a pulse and the vibrational oscillators. However, with large electric fields, multiple electric field−oscillator interactions can occur with a single pulse, resulting in fifth-order contributions to the echo emitted in the third-order phased-matched direction.

Previous, nominally third-order vibrational echo studies have identified contributions from fifth-order interactions. Fifth-order contributions led to the appearance of intensity-dependent oscillations in integrated vibrational echo signals of CO bound to hemoglobin.[14] The assignment of the observed oscillations to fifth-order origins was provided through experiments of CO bound to a myoglobin mutant H64V.[15] By spectrally resolving the vibrational echo signal in H64V experiments, a comparison could be made between the amplitudes of the oscillations at the 1−2 and 0−1 transition frequencies. The relative amplitudes and frequency dependence of the observed oscillations were well-explained by consideration of all fifth-order interaction pathways that lead to signals in the third-order phased-matched direction.

Special Issue: David W. Pratt Festschrift

Received: February 15, 2011
Revised: May 10, 2011
Published: June 07, 2011

These experiments were not heterodyne-detected; therefore, 2D spectra with diagonal and off-diagonal bands were not obtained, and the details of the time dependence of the fifth-order signals were not observed or explicated.

Since the previous reports, vibrational echo experiments are now routinely performed with heterodyne detection, providing the phase information for the generation of full 2D IR spectra.[16−19] Here, we report observations of fifth-order contributions in the 2D IR vibrational echo spectra of CO bound at the active site of the enzyme cytochrome $P450_{cam}$ with the substrate norcamphor (cyt P450-CO-norcamphor). The fifth-order contributions lead to the appearance of additional bands in the 2D IR spectra of cyt P450-CO-norcamphor separate from those arising from the third-order interactions. Of particular interest here are two bands, one of which is on the diagonal and one is off-diagonal. The frequency of these fifth-order bands is determined by the $v = 1-2$ transition frequency. These bands must be differentiated from bands due to other processes, such as chemical exchange, vibrational coupling, or energy transfer, which is one motivation for their characterization. In addition, the fifth-order bands display an unusual temporal dependence, decaying to 0 relatively quickly before reappearing with opposite sign. The diagonal band is initially positive, goes to 0, and then reappears as a negative band before finally decaying to 0. The off-diagonal band is initially negative. It decays to 0 and reappears as a positive band before decaying to 0. We explain the presence of these signals by consideration of the fifth-order Feynman interaction pathways and reproduce the temporal dependence of the fifth-order band amplitudes with model calculations that involve Feynman diagrams decaying into other diagrams.

2. MATERIALS AND METHODS

A. Sample Preparation. Cyt $P450_{cam}$ from *Pseudomonas putida* was produced by recombinant expression with plasmid pDNC-334A in *E. coli* strain NCM533[20] and purified as previously reported.[21,22] Experiments were performed with cyt $P450_{cam}$ C334A, which has been shown to display activity identical to wild-type but decreased propensity for aggregation.[23] To prepare the norcamphor complex, the sample was passed over Sephadex G25 in 50 mM Tris-MOPS, pH 7.4, 20% w/v glycerol, and exchanged by concentration and dilution into 50 mM sodium phosphate, pH 7.0, 100 mM KCl in D_2O, 20% w/v glycerol, containing 85 mM norcamphor.[24] The samples of the cyt P450-norcamphor complex were then concentrated to ~3 mM and clarified through 0.45 μm filters. The CO complexes were formed by reduction of the sample with 10-fold molar excess sodium dithionite, followed by exposure to a gentle stream of CO gas. The samples were placed between two CaF_2 windows with a 50 μm Teflon spacer. The UV/vis and linear FT IR spectra of the samples were recorded before and after 2D IR spectral acquisition to ensure sample integrity. Linear FT IR spectra were acquired at 1 cm^{-1} resolution on a Bruker Vertex 70 spectrometer. The linear IR spectra of samples studied with 2D IR spectroscopy showed CO bands of ~20 mOD on a ~0.35 OD background.

B. Vibrational Echo Spectroscopy. The time-resolved infrared experiments were performed as previously described[25,26] with 100 fs pulses at 1945 cm^{-1} generated with an ultrafast mid-IR laser system consisting of a Ti:Sapphire oscillator/regenerative amplifier pumped optical parametric amplifier. Briefly, the 2D IR echo experiments involve application of three separately

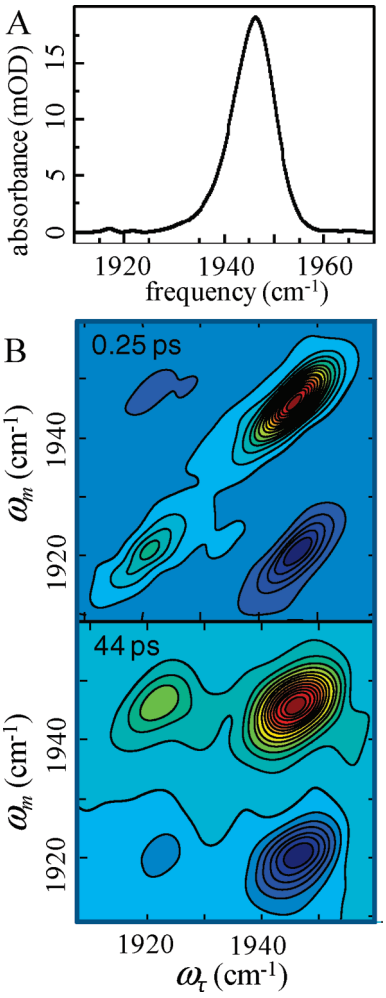

Figure 1. (A) Linear FT-IR spectrum of cyt P450-CO-norcamphor. (B) 2D IR spectra at short (0.25 ps, top panel) and long (44 ps, bottom panel) T_w times. The diagonal and off-diagonal peaks at $\omega_\tau = 1922$ cm^{-1} are due to fifth-order interactions. The signs of these peaks change between short and long time.

delayed pulses with wave vectors k_1, k_2, and k_3 to the sample in a boxcar geometry. Each excitation pulse had an energy of 1 μJ at the sample. The beams were focused to a spot size of 300 μm (99% diameter), yielding an energy density of ~20 GW/cm^2 at the sample for each pulse. The delay times between the arrival of the first and second pulses and the second and third pulses are referred to as τ and T_w, respectively.[25] At a time $\leq \tau$ after the third pulse, referred to as τ_s, a vibrational echo is emitted by the sample in the phase-matching $(-k_1 + k_2 + k_3)$ direction. The vibrational echo pulse is overlapped with another IR pulse, called the local oscillator, which provides a phase reference for the vibrational echo signal. The combined vibrational echo/local oscillator pulse is passed through a monochromator onto an IR array detector, which records a spectrum that yields the ω_m frequency axis (vertical axis), the axis of vibrational echo emission. For a fixed T_w (time between pulses 2 and 3), τ (time between pulses 1 and 2) is scanned to produce an interferogram at each ω_m. These interferograms are then Fourier transformed to produce the ω_τ axis (horizontal axis) of the 2D IR spectrum. T_w is then changed, and τ is again scanned to produce another 2D IR spectrum. The projection slice theorem was used to adjust the

spectral phase to obtain the absorptive 2D IR spectrum, as discussed previously.[25]

3. RESULTS/DISCUSSION

A. Experimental Vibrational Spectra. The linear FT-IR spectrum of cyt P450-CO-norcamphor shows a single Gaussian band with line width of 11 cm^{-1} centered at 1946 cm^{-1} (see Figure 1A), as has been observed in previous FT-IR studies of this protein.[24,27] Figure 1B displays 2D IR spectra of cyt P450-CO-norcamphor taken with short (250 fs, top panel) and long (44 ps, bottom panel) T_w times. In both spectra, an intense positive band appears along the diagonal at (ω_τ,ω_m) = (1946 cm^{-1},1946 cm^{-1}), which arises from the 0−1 vibrational transition. A negative band occurs for vibrational echo emission at the 1−2 transition frequency directly below the diagonal 0−1 band. This band is shifted along the ω_m axis by the vibrational anharmonicity (24 cm^{-1}) and is located at (ω_τ,ω_m) = (1946 cm^{-1},1922 cm^{-1}). For a single peak in the absorption spectrum, as is the case here (see Figure 1A), these two bands are the only bands that should appear in the 2D IR spectra for three-pulse vibrational echo experiments in which there is one field−matter interaction with each pulse, that is, for third-order experiments. The change in line shape of these bands when experiments are performed with varying T_w times reflects the spectral diffusion within the bands. The spectral diffusion for this system and for other substrates bound to cyt P450 has been analyzed in detail elsewhere.[28]

In addition to the third-order bands, two lower-amplitude bands also appear in the 2D IR spectra along a vertical line with ω_τ = 1922 cm^{-1} (Figure 1B). At the short T_w of 250 fs, a positive band occurs on the diagonal at (ω_τ,ω_m) = (1922 cm^{-1},1922 cm^{-1}), and a negative off-diagonal band occurs at (ω_τ,ω_m) = (1922 cm^{-1},1946 cm^{-1}). At the longer T_w time of 44 ps, these bands are still present but now have changed their signs. At first glance, the additional diagonal band might appear to reflect a second lower-frequency vibration, while the additional off-diagonal band might result from a third-order signal arising from processes such as chemical exchange, coupling, or vibrational energy transfer. However, these additional bands in Figure 1 arise from fifth-order interactions. The linear FT-IR spectrum of cyt P450-CO-norcamphor (Figure 1A) provides strong evidence for this assignment. While the 2D IR spectrum at T_w of 250 fs (Figure 1B) shows a relatively intense band at 1922 cm^{-1} on the diagonal, the linear FT-IR spectrum shows no absorption band at 1922 cm^{-1}. The absence of an absorption at 1922 cm^{-1} also means that the additional off-diagonal band at (ω_τ,ω_m) = (1922 cm^{-1},1946 cm^{-1}) cannot result from chemical exchange, coupling, or vibrational energy transfer as these processes require the participation of two vibrations. Furthermore, the additional bands do not appear in 2D IR spectra when experiments are performed with lower-intensity excitation pulses, as shown in the Supporting Information. Because of these observations, the additional bands are assigned to fifth-order signals. The fifth-order nature of these bands is demonstrated conclusively through the quantitative analysis presented below, which includes explication of the unusual time dependence in which the bands change signs at long time.

B. Theoretical Background. Theoretical methods for the calculation of nonlinear spectroscopic signals through the use of the response function formalism have been well-developed.[29]

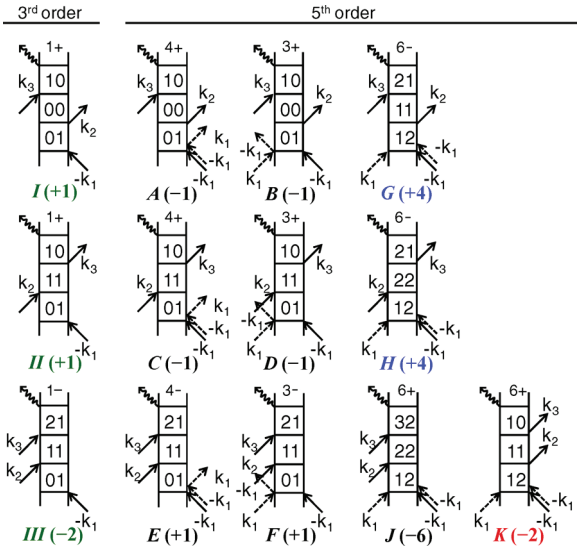

Figure 2. Diagrams of interaction pathways that contribute to third-order (left, I, II, and III) and fifth-order (right, A, B, C, D, E, F, G, H, J, and K) signals. Only fifth-order pathways involving three interactions within the first pulse are shown. Above each diagram are the sign and number of permutations of the incoming fields. Diagrams labeled in blue and red contribute to the diagonal and off-diagonal bands along ω_τ = 1922 cm^{-1}, respectively. In parentheses next to each label are the sign of the diagram's contribution to the 2D IR spectrum and the relative weight of the diagram's contribution arising from the different transition dipole moments of the transitions involved in the pathway.

Nonlinear spectroscopic signals arise from the macroscopic polarization generated in the sample by interactions with the applied optical electric fields. Three field−matter interactions lead to the generation of a third-order polarization, $P^{(3)}(t)$, which can be expressed by a convolution of the electric fields ($E_1(t)$, $E_2(t)$, $E_3(t)$) of the pulses with a response function ($R^T(t)$) that describes the material response to the applied fields.

$$P^{(3)}(t) = \int_0^\infty \int_0^\infty \int_0^\infty d\tau\, dT_w\, d\tau_s\, R^T(\tau_s, T_w, \tau) E_3(t-\tau_s) \times E_2(t-\tau_s-T_w) E_1(t-\tau_s-T_w-\tau) \quad (1)$$

R^T is a sum of contributions from all possible permutations of interactions of the light pulses with the sample.

Within the density matrix formalism, Feynman diagrams provide a pictorial representation for the field−matter interaction pathways and a convenient tool for explaining the signals observed in a nonlinear experiment.[29] While the total number of diagrams needed to represent all possible field−matter interaction pathways can be quite high, in practice, a smaller number are often required to understand a specific experiment. In conventional third-order vibrational echo spectroscopy, the signal arising in only the $-k_1+k_2+k_3$ direction is spatially filtered and detected. Thus, only those signals that arise from pulse combinations that result in emission in the $-k_1+k_2+k_3$ direction will contribute to the measured signal. In addition, only diagrams with temporally ordered, nonoverlapping pulses are considered. These are referred to as the echo or rephasing diagrams. For each rephasing diagram, there exists a nonrephasing diagram. Signals associated with these diagrams only occur when the separation in time of pulses 1 and 2 is less than the free induction decay time of the vibration. These diagrams produce signals at the same

frequencies and with the same signs as the rephasing diagrams, and their sum with the rephasing signals contributes to the absorptive 2D IR spectrum.[29] For the purposes of understanding the origins of the extra bands in Figure 1B and following their time dependence, consideration of only the rephasing diagrams is sufficient. The rotating wave approximation eliminates further pathways. With these considerations, description of the signals generated in a third-order vibrational echo experiment involving three energy levels (ground, first excited, and second excited vibrational states) requires three unique Feynman diagrams, which are shown in the first column of Figure 2 and are labeled I−III. In Figure 2, the Feynman diagram are constructed using common conventions; see ref 29 for details. The sign given above each diagram is obtained by $(-1)^n$, where n is the number of interactions from the right (bra). The number given above each diagram is the number of possible permutations of the incoming fields. In parentheses next to each diagram label is the sign of the contribution of the diagram to the resulting band in the 2D IR spectrum and a number that reflects the weighting of the diagram's contribution to the echo signal due to the involvement of 1−2 instead of 0−1 transitions in the interaction pathway (discussed further in section 3G, Model Calculations).

C. Third-Order Interaction Pathways. In all three third-order pathways, interaction with the first pulse brings the system into a coherence state (Figure 2). During the period before the arrival of the second pulse, the ensemble of oscillators undergoes dephasing for a time τ. Interaction with the second pulse creates a population state (either the ground or first excited state), in which the bra and ket are in the same state. The system evolves for the waiting time T_w. Finally, interaction with the third pulse again creates a coherence state where the system undergoes a rephasing period. At a time $t \geq \tau$ following this third pulse, the system can rephase and emit the vibrational echo signal. Fourier transformation of the interferograms generated by scanning τ leads to the ω_τ axis of the 2D IR spectrum. All three of the third-order diagrams involve a 0−1 coherence after the first pulse and lead to signals centered on ω_τ = 1946 cm^{-1} in the 2D IR spectrum. Diagrams I and II of Figure 2, which reflect the ground-state bleach and stimulated emission from the first excited state, respectively, will result in an echo signal at the 0−1 transition frequency (ω_m = 1946 cm^{-1}). Diagram III of Figure 2, which reflects excited-state absorption, will generate an echo signal at the 1−2 transition frequency (ω_m = 1922 cm^{-1}). Diagrams I and II of Figure 2 will lead to positive bands along the diagonal at (ω_τ,ω_m) = (1946 cm^{-1},1946 cm^{-1}) of the 2D IR spectrum. Diagram III of Figure 2 is opposite in sign and therefore results in a negative band at (ω_τ,ω_m) = (1946 cm^{-1},1922 cm^{-1}).

The amplitude of the emitted vibrational echo signal is strongly dependent on the laser pulse intensities as it varies with the product of the electric fields of the three laser pulses (E^3), that is, the emitted vibrational echo polarization is third-order in the electric field. However, in addition to increasing the third-order signal, the use of high-energy laser pulses increases the probability that the electric field will interact with the system more than once with at least one of the pulses. This can lead to the appearance of higher-order contributions to the signal generated in the direction of a nominally third-order experiment. In a centrosymmetric sample, that is, a liquid, the next-highest-order process that contributes to a nonlinear signal is fifth-order. The polarization generated in a fifth-order experiment is fifth-order in electric field, and therefore, the emitted signal varies as E^5. Fifth-order contributions have been previously observed by others in integrated vibrational echo signals and in frequency-resolved,but not heterodyne-detected vibrational echo signals.[14,15] In those previous studies, the fifth-order contributions were evident by the appearance of oscillations in the observed vibrational echo signal. The signs and time dependences of the signals were not examined. Presently, vibrational echo experiments are performed with heterodyne detection, which permits measurement of phase information and thus enables the generation of full 2D IR spectra. As discussed above, the fifth-order signals lead to the appearance of additional bands in the 2D IR spectrum.

D. Fifth-Order Interaction Pathways. Because the vibrational echo signal is measured in only the third-order phase-matching $-k_1 + k_2 + k_3$ direction, the two additional electric field interactions that result in fifth-order contributions cannot change the direction of the signal. Therefore, the two additional interactions must both occur within one pulse, and the wave vectors of the interacting fields must be opposite in sign. Figure 2 depicts the diagrams that can generate a signal in the phase-matching direction when the two additional interactions occur in the first pulse. In Figure 2, the additional interactions are represented by dashed arrows, and above each diagram, the number of permutations of the incoming fields and sign are given. In parentheses next to each diagram label (letter below the diagram) are the sign of the resulting band in the 2D IR spectrum and a number that reflects the weighting of the diagram's contribution to the echo signal due to the involvement of 1−2 instead of 0−1 transitions in the interaction pathway, as discussed in detail in section 3G, Model Calculations. Those diagrams where the two additional interactions both occur with either the bra or ket (diagrams A−F) leave the system in a state identical to the corresponding third-order diagrams at the end of the first pulse. Thus, these paths contribute to the third-order bands and do not produce additional bands. There are three interactions during pulse 1. The first puts the system into a 0−1 coherence state, the second takes the system into a 0 or 1 population state, and the third interaction returns the system to a 0−1 coherence state. The only difference between these fifth-order and third-order pathways is the additional population evolution period that occurs during the pulse. Due to the short duration of the excitation pulses (∼100 fs or shorter in many experiments), this additional very short population period will not influence the information content of the normal third-order 2D IR spectra generated from the experiments, as has been discussed more extensively in a previous publication.[15] Note, however, that the signs given above each diagram in Figure 2 are the same for the corresponding third- and fifth-order pathways. Because the total response function is multiplied by i^n, where n is the order of the experiment and i is the square root of −1, third- and fifth-order diagrams with the same sign lead to bands in the 2D IR spectrum with opposite sign. Therefore, fifth-order contributions from diagrams A−F to the mainly third-order bands are expected to result in a reduction in the observed amplitude of the third-order bands in 2D IR spectra.

For the cases in which the two additional interactions occur with one bra side and one ket side (diagrams G, H, J, and K of Figure 2), additional bands will appear in the 2D IR spectrum. Here, we are primarily interested in understanding the appearance of the bands found along ω_τ of the 1−2 transition frequency that may be mistaken for third-order signals (Figure 1). Because the pathways associated with these bands must include a 1−2 coherence during the dephasing period (following the first pulse), the contributing diagrams must show the additional

light−matter interactions in the first pulse. Diagrams G and H of Figure 2 lead to the emission of an echo signal at the 1−2 transition frequency and account for the initially positive 1−2 diagonal band at $(\omega_\tau,\omega_m) = (1922\ cm^{-1},1922\ cm^{-1})$. These diagrams are analogous to third-order diagrams I and II, but where the first two interactions in the first pulse initially put the system in the first excited state. Diagrams G and H reflect the bleach of the first excited state and stimulated emission from the second excited state, respectively. Diagram J of Figure 2 reflects excited-state absorption, analogous to third-order diagram II but from the second rather than first excited state. Diagram J leads to emission of an echo at the 2−3 transition frequency and a negative band shifted along ω_m from the positive diagonal bands from diagrams G and H. This band is outside of the frequency range of the 2D IR spectra shown in Figure 1, but an example 2D IR spectrum showing this band can be found in the Supporting Information. Diagram K is unique to the fifth-order response and has no analogous third-order pathway. It generates an echo at the 0−1 transition frequency and leads to the initially negative, off-diagonal band at $(\omega_\tau,\omega_m) = (1922\ cm^{-1},1946\ cm^{-1})$.

The nature of the pathways can be readily understood. Consider the G and H diagrams that give rise to the additional diagonal band. There are three radiation field−matter interactions in the first pulse. The first two populate the $v = 1$ vibrational level. Following these two interactions, the system is not different than if the 1 level had been populated thermally. The third interaction with the first pulse creates a 1−2 coherence state. The second pulse produces population states in both the 1 and 2 levels. The third pulse again produces a 1−2 coherence state with echo emission at the 1−2 transition frequency. Thus, after the first pulse, the system is in a 1−2 coherence state, yielding the ω_τ frequency of the 1−2 transition frequency. The last pulse again produces a 1−2 coherence state and vibrational echo emission at the 1−2 transition frequency. Therefore, the G and H pathways give rise to a diagonal band but with (ω_τ,ω_m) shifted from the 0−1 diagonal band by the vibrational anharmonicity.

The diagram J is the same as the G and H diagrams for the first two pulses. The third pulse takes the 2 level population state and produces a 2−3 coherence state and vibrational echo emission at the 2−3 transition frequency. In the same manner that the third-order 0−1 diagonal band has an off-diagonal band directly below it shifted to lower frequency along the ω_m axis by the anharmonicity, the 1−2 diagonal band has an off-diagonal band directly below it, also shifted to lower frequency along the ω_m axis by the anharmonicity. The K diagram gives rise to the off-diagonal band that is shifted along ω_τ to lower frequency by the vibrational anharmonicity (1−2 transition frequency) but has the 0−1 transition frequency on the ω_m axis. As before, the first two pulses involve four radiation field−matter interactions, three in the first pulse and one in the second pulse, leaving the system in the $v = 1$ population state. The third pulse creates a 1−0 coherence state with vibrational echo emission at the 0−1 transition frequency.

E. Lifetime Dependence of Third Order Signals. While at first glance the change in sign of the fifth-order bands as T_w increases seems strange, the observations can be accounted for by consideration of vibrational relaxation during the population periods recognizing that relaxation from $v = 2$ to 1 is approximately a factor of 2 faster than the relaxation from $v = 1$ to 0. In the harmonic approximation, the ratio of the lifetimes would be exactly a factor of 2.

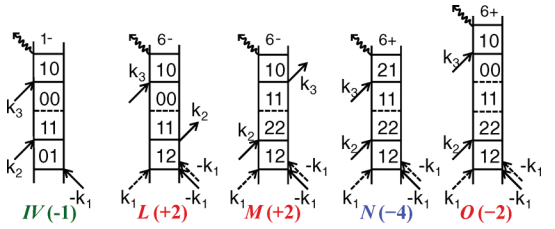

Figure 3. Diagrams including vibrational relaxation in the interaction pathways that contribute to the third-order (IV) and fifth-order (L, M, N, and O) vibrational echo signals. Vibrational relaxation is represented as a horizontal dashed line. Diagrams are labeled as those in Figure 2.

To clarify the issues, before treating the fifth-order bands, the time dependence of the third-order bands will be examined by following the changes in the contribution of the various interaction pathways as vibrational relaxation proceeds. To account for the initial amplitudes of these bands, one must consider both the number of pathways contributing to a signal and the transition dipole moments of the transitions involved in the pathways. The contribution of each pathway to a vibrational echo signal depends on the product of the transition dipole moments of the transitions involved in the pathway. In Figure 2, diagrams I and II involve only 0−1 transitions, while diagram III contains two 1−2 transitions. In the harmonic approximation, the 1−2 transition dipole is $\sqrt{2}$ greater than the 0−1 transition dipole. Thus, relative to diagrams I and II, diagram III results in 2-fold greater, $(\sqrt{2})^2$, signal amplitude. Two pathways (I and II) contribute to the 0−1 diagonal band, while only a single pathway (III) contributes to the off-diagonal band, but this single pathway produces a factor of 2 larger signal than the individual 0−1 pathways. The net result is that these third-order diagonal 0−1 and off-diagonal 1−2 bands have equal magnitudes but opposite signs.

An understanding of the decay of these third-order bands with increasing T_w can be gained by consideration of the result of vibrational relaxation during T_w in the diagrams I−III of Figure 2. Because the system is in the ground state during T_w in diagram I, vibrational relaxation cannot occur, and this diagram makes a positive contribution to the signal along the diagonal for all values of T_w. In contrast, vibrational relaxation will occur during T_w for diagrams II and III, leading to a ground-state population. Interaction with the third pulse can no longer result in stimulated emission, only induced absorption. Diagram IV of Figure 3 now describes the interaction pathway that contributes to the echo. In Figure 3, vibrational relaxation is represented by a horizontal dashed line. Diagram IV gives rise to a contribution to the vibrational echo emitted at the 0−1 frequency (diagonal band) and with negative amplitude. Diagram IV involves only 0−1 transitions, and therefore, the magnitude of its contribution is equal to that of diagram I. Thus, with increasing T_w, the positive contribution to the diagonal band from diagram II and the negative contribution to the off-diagonal band from diagram III decay, while a negative contribution to the diagonal band from diagram IV grows in with the exited-state lifetime. In the limit of long T_w, when vibrational relaxation is complete, the signals from diagrams II and III disappear, and the negative signal from diagram IV exactly cancels the positive signal from diagram I, leading to the decay of the 0−1 diagonal band. Thus, both the diagonal (0−1) and off-diagonal (1−2) third-order bands decay to 0 with the 1−0 vibrational lifetime, T_{10}.

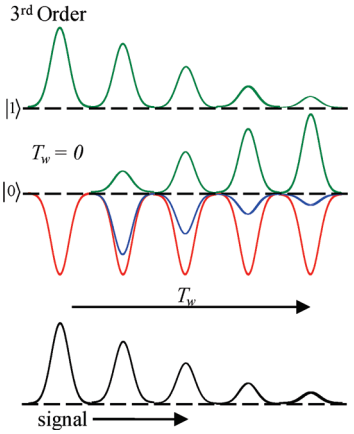

Figure 4. T_w dependence of the peak and hole in the populations of the vibrational levels involved in a third-order experiment. The green curves reflect the excess population (peak) generated in the 1 level that is transferred to the 0 level by vibrational relaxation. As the peaks in the 1 level decay, the resulting population in the 0 level is reflected by the green peaks in that level. The red curves show the reduced population (hole) generated in the 0 level, while the blue curves reflect the sum of the hole and peak in the 0 level. Both the 1 level peak and 0 level hole give positive contributions to the 0−1 diagonal band. The total signal with increasing T_w from the 1 level peak and 0 level hole (blue) contributions is illustrated in the black curves shown at the bottom of the figure.

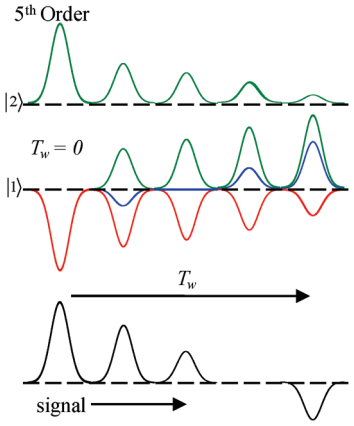

Figure 5. T_w dependence of peaks and holes in the populations of the vibrational levels involved in the fifth-order processes. As in Figure 4, the green curves reflect excess population (peak), the red curves reflect reduced population (hole), and the blue curves are the sum of the peak and hole in the 1 level at each time point. Both the 2 level peak and 1 level hole give positive contributions to the 1−2 diagonal band. Vibrational relaxation in the 2 level reduces the peak by the transfer of population from the 2 to the 1 level. This transfer of population fills in the 1 level hole at the same time that vibrational relaxation in the 1 level reduces the absolute size of the 1 level hole. At some point, the 1 level peak generated from vibrational relaxation out of the 2 level will exceed the size of the 1 level hole, and a net peak will exist in the 1 level (positive blue curve). At this point, the 1−2 diagonal band becomes negative. The total signal from the 2 level peak and 1 level hole (blue) contributions with increasing T_w is illustrated as the black curves shown at the bottom of the figure.

F. Lifetime Dependence of Fifth-Order Signals. An analogous treatment can be used to interpret the temporal changes in the intensity of the fifth-order bands with one major difference. Now, vibrational relaxation occurs from both the 2 and 1 levels, and their lifetimes differ by a factor of 2. As this paper is primarily interested in accounting for the additional bands observed along ω_τ = 1922 cm^{-1}, we focus the discussion on the time dependence of these bands, which are associated with diagrams G, H, J, and K in Figure 2. The signals of fifth-order diagrams A−F will display the same T_w dependence as the third-order diagrams to which they are nearly identical.

The fifth-order diagrams L−O that result when vibrational relaxation is included during T_w are given in Figure 3. Vibrational relaxation during T_w in diagrams G and K leads to a ground-state population. As only induced absorption, not stimulated emission, can occur from the ground state, diagrams G and K become only one diagram, diagram L of Figure 3. The echo of diagram L emits at the 0−1 frequency, leading to a positive off-diagonal band at ω_τ and ω_m of the 1−2 and 0−1 frequencies, respectively. Because the ground-state population cannot further relax, the positive signal contribution by diagram L persists for all longer T_w's.

Vibrational relaxation from the second excited state during T_w in diagrams H and J leads to a first excited state level population. The third pulse now results in diagrams M and N of Figure 3. The echo from diagram M emits at the 0−1 frequency, leading to a positive off-diagonal band at ω_τ and ω_m of the 1−2 and 0−1 frequencies, respectively. The echo of diagram *N* emits at the 1−2 frequency, leading to a negative contribution of the band at the 1−2 diagonal. Further vibrational relaxation from the first excited state during T_w leads to a ground-state population. Now, the third pulse may only induce absorption, as represented by diagram O. The echo of diagram O emits at the 0−1 frequency and leads to a negative contribution to the off-diagonal fifth-order band. Because the ground-state population cannot relax further, the negative signal contribution from diagram O persists for all longer T_w times.

Before quantitatively describing the time dependence of the fifth-order signals, the mechanism for the change in sign of the signals with increasing T_w embodied in the diagrammatic description will be described qualitatively for the fifth-order diagonal band. First, consider the normal third-order 0−1 diagonal band. After the first two interactions (first two pulses), there are populations in the 1 state and in the 0 state that have been prepared by the pulses. Figure 4 illustrates the T_w dependence of the populations and the resulting 0−1 diagonal band amplitude. An increase in population will be called a peak (green curves), and a reduction in population will be called a hole (red curves). The hole gives a positive contribution to the 0−1 signal because it is a bleach, that is, a reduction in absorption, seen by the third pulse. The peak also gives a positive contribution from stimulated emission induced by the third pulse. As T_w increases, vibrational relaxation leads to transfer of population from the 1 level to the 0 level (depicted by the transfer of amplitude of the green curves from 1 to 0). Vibrational relaxation cannot occur out of the 0 level; therefore, the initially generated hole contribution remains constant (red curves) . As the peaks in the 1 level decay, the transferred population fills the 0 level holes, which is depicted as reduction in amplitude of the blue curves. The blue curves are the sum of the 0 level peaks (green) and the 0 level holes (red). The signal results from contributions from the 1 level peak (green) and the 0 level hole (blue). Both are positive. The combination of these contributions to the signal is reflected in the black curves in Figure 4. Both the peak and hole contributions to the signal, and consequently the 0−1 diagonal band, decay together.

dx.doi.org/10.1021/jp201516s |*J. Phys. Chem. A* 2011, 115, 9714–9723

The T_w dependence of the populations that lead to the changes in the amplitude of the fifth-order 1−2 diagonal band is illustrated in Figure 5. There are three interactions in the first pulse. The first two interactions in the first pulse produce population in the 1 level. The last interaction in the first pulse and the interaction with the second pulse produce a peak in the 2 state (green) and a hole in the 1 state population (red) that was created by the first two interactions in the first pulse (far left, Figure 5). The 2 state peak and the 1 state hole both give positive contributions to the diagonal 1−2 band. Vibrational relaxation from the 2 state to the 1 state reduces the 2 state peak, and its positive contribution to the 1−2 diagonal band decays with time constant T_{21} (green curves in 2 level, Figure 5). Vibrational relaxation also occurs out of the 1 state and reduces the hole by reducing the total population in the 1 state with time constant T_{10} (red curves, Figure 5). This is in contrast to the 0 state holes in Figure 4 that cannot decay by relaxation to a lower energy level. Thus, the 1 state hole is reduced due to vibrational relaxation out of the 1 state at the same time that it is filled by vibrational relaxation from the 2 level. In Figure 5, the blue curves in the 1 level are the sum of the 1 level green curves produced by relaxation of the 2 level peak population and red curves reflecting the size of the 1 level hole. Because the 1 state population is relaxing to the 0 state and reducing the absolute size of the hole, it does not require all of the 2 state population to relax into the 1 state to fill the hole. At some point, the hole will be filled completely with some of the 2 state peak still in existence. The absence of a hole is shown in the middle of Figure 5 as the horizontal blue line showing zero amplitude. At this point, the signal is still positive. There is no contribution from the 1 state because the hole is filled, but there is stimulated emission from the 2 state induced by the third pulse, as shown by the fact that there is still a green peak in the 2 state. Further relaxation from the 2 state to the 1 state forms a peak in the 1 state where previously there had been a hole. This peak is shown as the positive-going blue curve. The peak in the 1 state looks like a new absorption to the third pulse; therefore, it makes a negative contribution to the signal. When the positive contribution from the 2 level peak and the negative contribution from the newly formed 1 level peak are equal, the amplitude of the 1−2 diagonal band is 0 (set of curves second from the right in Figure 5). A negative 1−2 band then grows in as the 1 level curves (blue curve) becomes increasingly greater than the remaining 2 level peak (green curve) with further increase in T_w (far right, Figure 5). The negative signal arising from the absorptive peak in the 1 state then decays to 0 with the 1 level lifetime T_{10}. Therefore, Figure 5 shows schematically that the signal starts positive, goes to 0, and then grows back in negative.

G. Model Calculations. The following schemes describe the T_w dependence of the contributions of the Feynman diagrams to the 2D IR spectra.

$$\text{G and K} \xrightarrow{T_{10}} \text{L} \qquad \text{H and J} \xrightarrow{T_{21}} \text{M and N} \xrightarrow{T_{10}} \text{O}$$

T_{10} is the vibrational lifetime for relaxation from the 1 state to the 0 state, and T_{21} is the vibrational lifetime for relaxation from the 2 state to the 1 state. In the calculations, $T_{21} = T_{10}/2$.

Solving the system of rate equations for the changes in the contributions of the interaction pathways with T_w shown above yields the following equations

$$P_{G,K}(T_w) = e^{-T_w/T_{10}} \tag{2a}$$

$$P_L(T_w) = 1 - e^{-T_w/T_{10}} \tag{2b}$$

$$P_{H,J}(T_w) = e^{-T_w/T_{21}} \tag{2c}$$

$$P_{M,N}(T_w) = \left(\frac{T_{10}}{T_{21} - T_{10}}\right)(e^{-T_w/T_{21}} - e^{-T_w/T_{10}}) \tag{2d}$$

$$P_O(T_w) = \left(\frac{1}{T_{21} - T_{10}}\right)(T_{21}e^{-T_w/T_{21}} + T_{10}e^{-T_w/T_{10}} + T_{21} + T_{10}) \tag{2e}$$

For all diagrams contributing to the signals along ω_τ of the 1−2 transition (i.e., diagrams G−K of Figure 2 and L−O of Figure 3), there are six possible permutations of the incoming pulses (given at the top of each diagram). Therefore, each diagram contributes equally to the signal. However, the contribution of each pathway to an echo signal also depends on the product of the transition dipole moments of the transitions involved in the pathway. Diagrams G, H, and N involve four 1−2 transitions, while diagrams K, L, N, and O involve two. In the harmonic approximation, the 1−2 transition dipole is $\sqrt{2}$ larger than the 0−1 transition dipole. Then, compared to fifth-order diagrams A−F containing only 0−1 transitions, diagrams G, H, and N yield signals 4-fold greater in amplitude, and diagrams K, L, N, and O yield signals 2-fold greater in amplitude, that is, $(\sqrt{2})^4$ and $(\sqrt{2})^2$, respectively. Therefore, 2-fold greater signal arises from each of the diagrams G, H, and N that give rise to the 1−2 diagonal band compared to diagrams K, L, N, and O associated with the off-diagonal band. At the earliest T_w's, the 1−2 diagonal band is expected to be 4-fold greater in amplitude than the off-diagonal band because two pathways (G and H) contribute 2-fold greater amplitude to the 1−2 diagonal band, while only one pathway (K) contributes to the off-diagonal band.

Of particular importance are the signs of the diagrams that contribute to the diagonal and off-diagonal bands along ω_τ = 1922 cm^{-1}. As discussed qualitatively in connection with Figure 5, as T_w increases, the amplitude associated with the diagrams that contribute to the various peaks change. From consideration of these diagrams, the origin of the changing signs of the fifth-order bands with increasing T_w becomes clear. At earliest T_w times, the diagonal and off-diagonal bands are positive and negative, respectively, with a 4/1 amplitude ratio. For the 1−2 diagonal band, vibrational relaxation from the first excited state reduces the contribution of diagram G and thus leads to the decay of half of the initial positive amplitude to 0 with time constant T_{10} at long time. Vibrational relaxation from the second excited state reduces the contribution from diagram H, and the second half of the initial positive amplitude of the 1−2 diagonal band decays to 0 at long time with time constant T_{21}. At the same time, the vibrational relaxation from the second to the first excited state generates a contribution from diagram N, leading to the growth of a negative band with time constant T_{21}. This negative contribution then decays to 0 with time constant T_{10} as vibrational relaxation reduces the first-excited-state population during T_w.

The temporal variation in the off-diagonal band along ω_τ = 1922 cm^{-1} can be explained in a similar manner. As vibrational relaxation from the first excited state proceeds, the initial negative off-diagonal band due to diagram K decays to 0 with time constant T_{10}. At the same time, a positive contribution to the

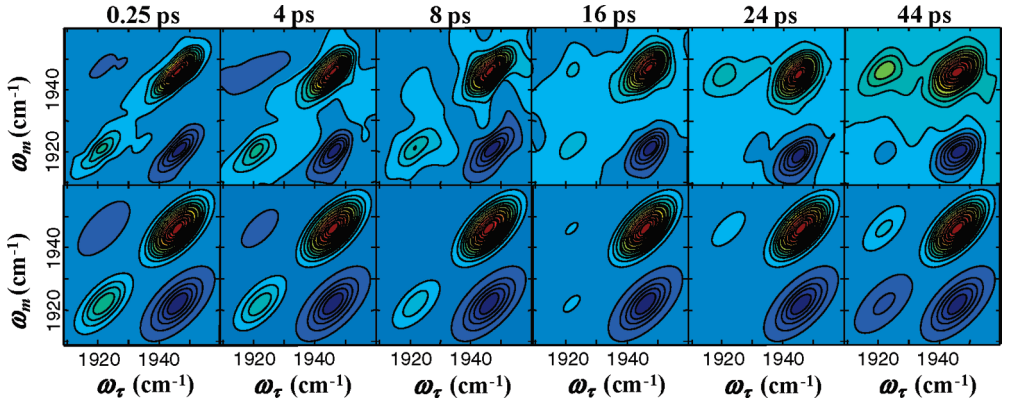

Figure 6. Experimental (upper panels) and calculated (lower panels) 2D IR vibrational echo spectra at varying T_w times. 20 contour lines are shown in each 2D IR spectrum. The calculations reproduce the diagonal and off-diagonal fifth-order peaks at ω_τ = 1922 cm^{-1}, and they replicate the time dependence including the decay of the fifth-order peaks to 0 and their re-emergence with opposite sign as T_w is increased.

off-diagonal band from diagram L grows in. For longer T_w times, the positive contribution from diagram L remains constant. Simultaneous with the vibration relaxation from the 1 level to the ground state of diagrams G and K, vibrational relaxation from the 2 level to the 1 level of diagrams H and J leads to the appearance of diagram M, generating a positive contribution to the off-diagonal band with time constant T_{21}. With time constant T_{10}, this positive contribution then disappears, and a negative contribution from diagram O appears as vibrational relaxation brings population from the first excited state to the ground state. For longer T_w times, the negative contribution from diagram O remains constant. In the limit of long T_w, the constant positive contribution from diagram L and the constant negative contribution from O exactly cancel, and the off-diagonal band has decayed to 0.

Considering eq 2 describing the T_w-dependent population of the fifth-order diagrams, as well as the magnitudes and signs of the resulting signals, the following equations describing the T_w-dependence of the amplitudes of the fifth-order bands along ω_τ = 1922 cm^{-1} can be derived

$$A_{12/01}(T_w) = -P_K(T_w) + P_L(T_w) + P_M(T_w) - P_O(T_w) \quad (3a)$$

$$A_{12/12}(T_w) = 2P_G(T_w) + 2P_H(T_w) - 2P_N(T_w) \quad (3b)$$

Using these equations, the changes in the relative amplitudes of the bands in the 2D IR spectra with increasing T_w were calculated. The experimental band shapes change to some extent as T_w is increased because of spectral diffusion. Spectral diffusion does not change the volumes of the peaks.[8,30] Spectral diffusion was not included in the calculations as the aim here is to account for the time-dependent amplitudes and signs of the bands. In the calculations, 2D Gaussian functions with constant line widths both along the diagonal and perpendicular to the diagonal were used to model the bands for all T_w. The amplitudes of the Gaussian functions (the volume of the band) at each T_w were set according to the signal intensity given by eq 3.

The amplitudes of the bands along ω_τ = 1946 cm^{-1} are the sum of the third-order contributions and smaller fifth-order contributions of opposite sign from diagrams A−F (as well as diagrams involving multiple interactions in the second and third pulses). All contributions decay with the 1 level lifetime, T_{10}. In the presentations of the experimental data and the calculated spectra (Figure 6), the diagonal nominally third-order band at (1946 cm^{-1},1946 cm^{-1}) is normalized to 1 at each time. The amplitudes of the other bands are relative to the diagonal third-order band. As the initial relative intensities of the fifth-order diagonal band at ω_τ = 1922 cm^{-1} and third-order diagonal band at ω_τ = 1946 cm^{-1} will depend on the pulse intensities, the spectra of the excitation pulses, and other experimental factors, the initial intensities of these two bands were a match to their experimental values at the shortest T_w, 0.25 ps. The initial ratio of the fifth-order diagonal band to the third-order diagonal band is 1/6. The relative amplitudes of the other bands at a T_w of 0.25 ps are based on the calculations. At all other T_w's, the amplitudes of all of the bands are calculated as changes from their initial values. The bands at ω_τ = 1946 cm^{-1} were then set to decay with a time constant T_{10}, which was independently measured to be 20 ps for cyt P450-CO-norcamphor. T_{21} was taken to be 10 ps, half of the first excited vibrational state lifetime, which is in accord with the harmonic approximation.

Figure 6 shows a comparison of the experimentally determined (upper panels) and calculated (lower panels) changes in the 2D IR spectra of cyt P450-CO-norcamphor with increasing T_w. The experimental spectra are reproduced well by the model calculations. In both sets of spectra, the negative off-diagonal band at (ω_τ,ω_m) = (1922 cm^{-1},1946 cm^{-1}) decays to 0 by a T_w of ∼8 ps and then reappears with positive sign by ∼16 ps. The positive diagonal band at (ω_τ,ω_m) = (1922 cm^{-1},1922 cm^{-1}) decays to 0 by a T_w of ∼24 ps and then reappears with negative sign by ∼44 ps. The fact that the time dependences of the bands are well described by the standard theoretical treatment of nonlinear spectroscopy strongly supports the assignment of the bands as fifth-order signals. The close agreement also suggests that our use of the harmonic approximations for the transition dipole of the 1−2 transition and the lifetime of the second excited state are reasonable. The value of T_{21} used for calculating the T_w-dependent changes could be varied between 10 and 13 ps, and similar T_w dependences of the band amplitudes were observed.

The dynamics of cyt P450 in various substrate complexes from analysis of the third-order bands is reported elsewhere.[28] Qualitatively, however, the changes in the line shapes of the fifth-order bands with increasing T_w appear similar to those of the third-order bands (see Figure 6 upper panels). The off-diagonal

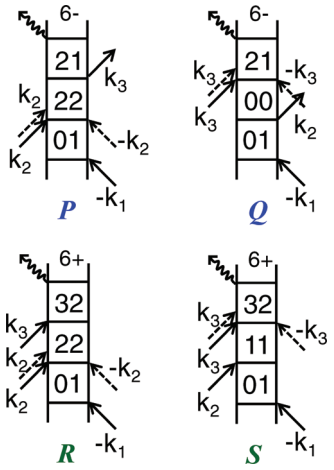

Figure 7. Fifth-order diagrams involving three interactions in either the second or third pulses that reflect pathways that differ substantially from the third-order pathways.

band along ω_τ = 1922 cm^{-1} arises only from diagrams that involve a ground-state or first-excited-state population during T_w. Thus, the dynamics reflected in the line shapes of this band are not expected to differ substantially from those arising from the third-order pathways. The 1−2 diagonal band, however, originates partially from a pathway involving a second-excited-state population (diagram H, Figure 2). Dynamics on the second-excited-state surface, as well as on the ground and first excited states, therefore contribute to the T_w dependent changes in the line shape of this band. A better characterization of the dynamics on the second-excited-state surface could be gained through analysis of the line shape of the band that is generated from the pathway given in diagram K in Figure 2, which involves only the second excited state during the population period T_w.

As the primary goal of this paper was the identification and theoretical explanation of the T_w-dependent additional bands observed in the 2D IR spectra along ω_τ = 1922 cm^{-1}, we have focused our attention on the fifth-order pathways involving three interactions with the first pulse. Although pathways with multiple interactions with the second and third pulses do not result in bands along ω_τ = 1922 cm^{-1}, they do generate fifth-order signals elsewhere in the spectra. Like the diagrams A−F of Figure 2 discussed above, one can generate fifth-order diagrams where two additional interactions occur with the second or third pulses, both with either the bra or ket.[15] In these cases, the diagrams are nearly equivalent to those of the third-order pathways, but the resulting 2D IR bands are opposite in sign from the corresponding third-order bands. Thus, increasing laser intensity will only increase the amplitude of the third-order 2D IR bands to a certain extent before generation of fifth-order signals on top of them will start reducing the magnitude of the increase expected from increasing the laser intensity.

Finally, when two additional interactions occur with the second and third pulses and each pulse interacts with either the bra or ket, the interaction pathways do not lead to additional bands along ω_τ = 1922 cm^{-1}, but one band appears on top of the off-diagonal third-order band and another appears at ω_τ and ω_m of the 0−1 and 2−3 transition frequencies, respectively. The diagrams for these signals are given in Figure 7. Diagrams P and Q lead to bands with positive amplitude, which overlap and diminish the observed amplitude of the negative 1−2 off-diagonal third-order band. Thus, fifth-order signals result in the 2D IR spectra displaying a positive diagonal 0−1 band and a negative off-diagonal 0−1 band of unequal magnitude, with the off-diagonal band smaller relative to the diagonal band. Diagrams R and S will lead to a negative band at ω_m of the 2−3 transition frequency, which is beyond the frequency limits of the spectra shown in Figures 1 and 6. A spectrum that shows all of the bands is given in Supporting Information.

In this study, we have pointed out the fifth-order signals that appear in nominally third-order spectra. Other researchers have designed experiments for measuring fifth-order signals. For example, Zanni and others employ a three-pulse experiment to look at fifth-order signals that emit in a distinct direction, $-2k_1 + k_2 + 2k_3$.[31] The fifth-order signals discussed here are emitted in the third-order phase-matching direction.

4. CONCLUDING REMARKS

Two bands, one diagonal and one off-diagonal, are observed along ω_τ = 1922 cm^{-1} in 2D IR vibrational echo spectra of cyt P450-CO-norcamphor. This frequency is shifted to lower frequency along ω_τ compared to the main diagonal third-order band by the vibrational anharmonicity. The amplitudes of these bands are T_w-dependent and change sign at sufficiently long T_w. The results presented above have demonstrated that these bands are due to fifth-order signals that are emitted in the third-order phase-matched direction. The nature of these fifth-order bands can be explained using standard theoretical methods. We have calculated the temporal dependence of the amplitudes of the fifth-order bands by accounting for the influence of vibrational relaxation on the contributing interaction pathways. The unusual time dependence, in which the bands go relatively rapidly to 0 and then reappear with opposite sign, is caused by the fact that the vibrational relaxation from the second vibrationally excited state to the first vibrationally excited state is substantially faster (approximately a factor of 2 faster) than relaxation from the first vibrationally excited state to the ground state. The close correspondence of the experimental and calculated spectra validates our assignment of the additional bands to fifth-order origins. The data demonstrate that analysis of spectra presumed to result from third-order interactions must be performed with caution. Positive, off-diagonal bands due to other processes such as chemical exchange and vibrational energy transfer may appear on a time scale similar to that of the fifth-order bands observed in the spectra reported here.

It is also worth noting the effect that the fifth-order processes delineated here can have on the time dependence of IR pump−probe experiments. The pump−probe signal is the projection of the 2D IR spectrum onto the ω_m axis (see Figures 1 and 6). The signal is integrated along the ω_τ axis. Thus, fifth-order bands will be mixed in with the normal pump−probe third-order bands if sufficiently high pump power is used. In the 2D IR spectra, the fifth-order bands are distinct, and their time dependence is manifested independent of the normal third-order bands. However, in the pump−probe experiment, the time dependence of the fifth-order bands, as they go rapidly to 0, change sign, and grow back in, will appear as part of the pump−probe time dependence. It is possible that an exponential decay at low power will appear nonexponential with a time dependence determined, in part, by the time dependence of the fifth-order bands explicated here.

■ ASSOCIATED CONTENT

Supporting Information. Intensity Dependence of Fifth-Order Bands. This material is available free of charge via the Internet at http://pubs.acs.org.

■ AUTHOR INFORMATION

Corresponding Author
*E-mail: fayer@stanford.edu.

■ ACKNOWLEDGMENT

We would like to thank Professor Shaul Mukamel, Department of Chemistry, University of California at Irvine, for a useful discussion of this work. This work was supported by National Institutes of Health (2-R01-GM061137-09) and the National Science Foundation (DMR 0652232). M.C.T. acknowledges the support of a Ruth L. Kirschstein National Research Service Award administered through the National Institutes of Health (F32-GM090549).

■ REFERENCES

(1) Rector, K. D.; Kwok, A. S.; Ferrante, C.; Tokmakoff, A.; Rella, C. W.; Fayer, M. D. *J. Chem. Phys.* **1997**, *106*, 10027.
(2) Golonzka, O.; Khalil, M.; Demirdoven, N.; Tokmakoff, A. *Phys. Rev. Lett.* **2001**, *86*, 2154.
(3) Zanni, M. T.; Hochstrasser, R. M. *Curr. Opin. Struct. Biol.* **2001**, *11*, 516.
(4) Roberts, S. T.; Loparo, J. J.; Tokmakoff, A. *J. Chem. Phys.* **2006**, *125*, 084502.
(5) Kwak, K.; Rosenfeld, D. E.; Fayer, M. D. *J. Chem. Phys.* **2008**, *128*, 204505.
(6) Kwak, K.; Park, S.; Finkelstein, I. J.; Fayer, M. D. *J. Chem. Phys.* **2007**, *127*, 124503.
(7) Fayer, M. D. *Annu. Rev. Phys. Chem.* **2009**, *60*, 21.
(8) Zheng, J.; Kwak, K.; Asbury, J. B.; Chen, X.; Piletic, I.; Fayer, M. D. *Science* **2005**, *309*, 1338.
(9) Zheng, J.; Kwak, K.; Xie, J.; Fayer, M. D. *Science* **2006**, 1951.
(10) Moilanen, D. E.; Wong, D. B.; Rosenfeld, D. E.; Fenn, E. E.; Fayer, M. D. *Proc. Natl. Acad. Sci. U.S.A.* **2009**, *106*, 375.
(11) Rosenfeld, D. E.; Kwak, K.; Gengeliczki, Z.; Fayer, M. D. *J. Phys. Chem. B* **2010**, *114*, 2383.
(12) Khalil, M.; Demirdoven, N.; Tokmakoff, A. *J. Chem. Phys.* **2004**, *121*, 362.
(13) Kurochkin, D. V.; Naraharisetty, S. R. G.; Rubtsov, I. V. *Proc. Natl. Acad. Sci. U.S.A.* **2007**, *104*, 14209.
(14) Hamm, P.; Lim, M.; Asplund, M.; Hochstrasser, R. M. *Chem. Phys. Lett.* **1999**, *301*, 167.
(15) Finkelstein, I. J.; McClain, B. L.; Fayer, M. D. *J. Chem. Phys.* **2004**, *121*, 877.
(16) Zanni, M. T.; Gnanakaran, S.; Stenger, J.; Hochstrasser, R. M. *J. Phys. Chem. B* **2001**, *105*, 6520.
(17) Asplund, M. C.; Zanni, M. T.; Hochstrasser, R. M. *Proc. Natl. Acad. Sci. U.S.A.* **2000**, *97*, 8219.
(18) Hamm, P.; Lim, M.; DeGrado, W. F.; Hochstrasser, R. M. *Proc. Natl. Acad. Sci. U.S.A.* **1999**, *96*, 2036.
(19) Asbury, J. B.; Steinel, T.; Stromberg, C.; Gaffney, K. J.; Piletic, I. R.; Goun, A.; Fayer, M. D. *Phys. Rev. Lett.* **2003**, *91*, 237402.
(20) Hamuro, Y.; Molnar, K.; Coales, S.; Ouyang, B.; Simorellis, A.; Pochapsky, T. *J. Inorg. Biochem.* **2008**, *102*, 364.
(21) O'Keefe, D. H.; Ebel, R. E.; Peterson, J. A. *Methods Enzymol.* **1978**, *103*, 151.
(22) Unger, B. P.; Gunsalus, I. C.; Sligar, S. G. *J. Biol. Chem.* **1986**, *261*, 1158.
(23) Nickerson, D. P.; Wong, L. L. *Protein Eng.* **1997**, *10*, 1357.
(24) Jung, C.; Bon Hoa, G. H.; Schroeder, K. L.; Simon, M.; Doucet, J. P. *Biochemistry* **1992**, *31*, 12855.
(25) Park, S.; Kwak, K.; Fayer, M. D. *Laser Phys. Lett.* **2007**, *4*, 704.
(26) Fenn, E. E.; Wong, D. B.; Fayer, M. D. *J. Chem. Phys.* **2011**, *134*, 054512.
(27) Jung, C.; Schulze, H.; Deprez, E. *Biochemistry* **1996**, *35*, 15088.
(28) Thielges, M. C.; Chung, J. K.; Fayer, M. D. *J. Am. Chem. Soc.* **2011**, *133*, 3995.
(29) Mukamel, S. *Principles of Nonlinear Optical Spectroscopy*; Oxford University Press: New York, 1995.
(30) Kwak, K.; Zheng, J.; Cang, H.; Fayer, M. D. *J. Phys. Chem. B* **2006**, *110*, 19998.
(31) Ding, F.; Fulmer, E.; Zanni, M. T. *J. Chem. Phys.* **2005**, *123*, 094502.